Journal of Materials Research and Technology 42 (2026) 1224–1228

Contents lists available at ScienceDirect

Journal of Materials Research and Technology

journal homepage: www.elsevier.com/locate/jmrt

In situ and locally resolved analysis of retained austenite stability during tensile loading in a high-strength weld metal

Daniel Schrittwieser [a,*], Benjamin Seligmann [a], David Obersteiner [a], Sabine C. Bodner [a], Hannes Pahr [b], Oleksandr Glushko [a], Ronald Schnitzer [a]

[a] Department of Materials Science, Technical University of Leoben, Franz Josef-Straße 18, 8700 Leoben, Austria
[b] voestalpine Böhler Welding Austria GmbH, Böhler-Welding-Straße 1, 8605 Kapfenberg, Austria

ARTICLE INFO

Keywords:
Welding
In situ high-energy X-ray diffraction
Strain-induced phase transformation
Retained austenite
High-strength weld metal
Tensile test

ABSTRACT

The transformation of retained austenite under mechanical load has a significant impact on the mechanical properties of high-strength low-alloy steels and weld metals. Here, we have studied the stability of retained austenite in a microalloyed, multipass high-strength all-weld metal using *in situ* high-energy X-ray diffraction phase quantification during tensile loading. Two-dimensional phase maps were acquired before and after testing to reveal the locally resolved distribution of strain-induced austenite transformation. Depending on the position within the unstrained specimen, the amount of retained austenite varied between 1 wt.% and 6 wt.%. During loading, the retained austenite remained largely mechanically stable within the macroscopic elastic regime. Upon the onset of plastic deformation, a pronounced transformation of the metastable retained austenite occurred. Plastic deformation was predominantly localized in areas which were not reheated during multipass welding. In regions where reheating occurred, precipitation hardening from microalloying elements produced a microstructure with significantly higher strength levels.

1. Introduction

Retained austenite (RA) is a decisive phase in steels that strongly influences their mechanical properties [1]. Understanding the specific behavior of this metastable phase across different steel grades under various environmental and loading conditions is therefore essential. A key factor defining the behavior of RA within the microstructure is its stability, which depends primarily on chemical composition, size, morphology, and the strain distribution within adjacent microstructural constituents [2]. In advanced high-strength steels exploiting the transformation-induced plasticity (TRIP) effect, C segregation to the austenitic phase is intentionally promoted by alloying and optimized heat treatments to stabilize a target fraction of RA down to room temperature [3,4]. As an example, Qi et al. [5] reported a higher stability of RA with increasing C and Mn enrichment in a medium-Mn steel. Considering the influence of morphology on the stability of RA in low-alloy steel grades, it is well established that blocky RA is less stable than film-like RA. Moreover, blocky RA tends to transform into martensite at relatively low stresses, which detrimentally affects strength and toughness [6–8]. Consequently, many studies focus on heat treatments or alloying strategies to intentionally form film-like RA [9–11]. Bhadeshia and Edmonds [7] even addressed this topic quantitatively and reported that the ratio of the volume fraction of stable film-like to unstable blocky RA must exceed 0.9 to achieve optimum mechanical properties in low-alloy bainitic steels.

In high-strength weld metals and the heat-affected zone of high-strength low-alloy steels, RA is typically only considered as part of martensite-austenite constituents, owing to their significant influence on mechanical properties [12–16]. However, our recent study [17] has shown that up to 7 wt.% of RA can be locally present within multipass high-strength weld metals both as part of martensite-austenite constituents but also as stand-alone phase. Previous studies on high-strength steels and weld metals have often underestimated this considerable amount due to investigation methods that were limited to surface analysis and the corresponding challenges of sample preparation [17–19]. Building on the ability of high-energy X-ray diffraction (HEXRD) to accurately quantify RA based on information from a large sample volume, and thus without being affected by surface conditions and sample preparation, the present study advances this understanding by analyzing the stability of RA in a multipass high-strength weld metal.

* Corresponding author.
E-mail address: daniel.schrittwieser@unileoben.ac.at (D. Schrittwieser).

https://doi.org/10.1016/j.jmrt.2026.03.159
Received 26 February 2026; Received in revised form 12 March 2026; Accepted 17 March 2026
Available online 18 March 2026

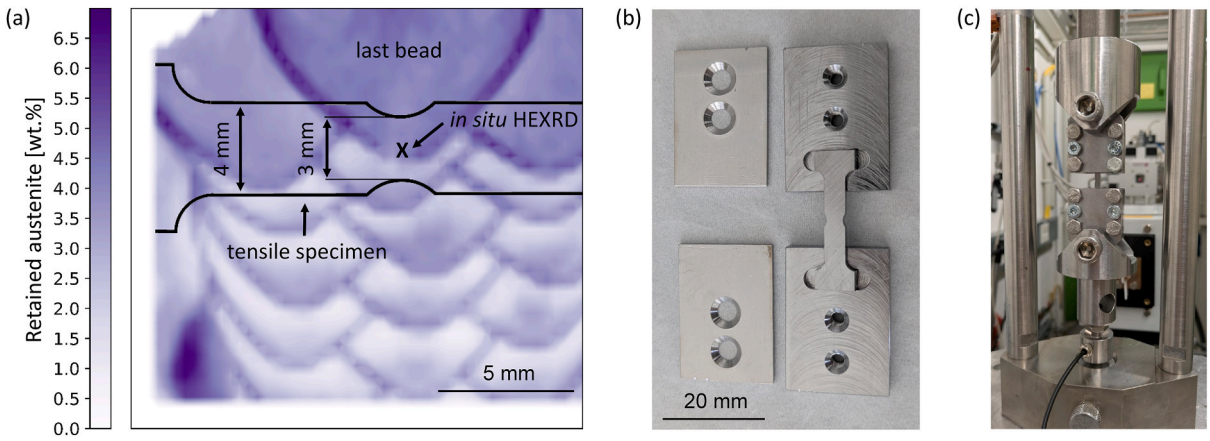

Fig. 1. a) RA phase map of the multipass high-strength weld metal derived from data of Reference [17], showing the position of the extracted tensile specimen and the X-ray beam location for the *in situ* HEXRD investigation. **b)** Tensile specimen with the corresponding adaptor. **c)** Tensile testing machine at the synchrotron facility.

A tensile test was performed on a specimen extracted from the same weld metal investigated by the authors in Reference [17], with simultaneous HEXRD measurements to analyze the stability of RA *in situ*. In addition, two-dimensional HEXRD mappings were conducted before and after testing to obtain locally resolved information on the behavior of RA following deformation.

2. Methods

The investigated multipass weld metal was produced via gas metal arc welding and comprises seven layers with three beads per layer. The chemical composition is Fe-0.09C-0.5Si-1.5Mn-0.6Cr-0.5Mo-2.9Ni-0.2V (wt.%) and the minimum yield strength is 1100 MPa in the multipass welded condition. For further details about the welding procedure and the microstructure the reader is referred to Reference [17]. The distribution of RA across the multipass weld metal (derived from data of Reference [17]) is given in Fig. 1a) together with the location of the tensile specimen, which is 2.5 mm thick and 4 mm wide along most of its length, narrowing to 3 mm at the notch. The geometry of the specimen was designed such that the width of 3 mm is present exactly at the location of the *in situ* HEXRD measurement, enabling the observation of plastic deformation. Consequently, no strain can be determined from the tensile test, as no gauge length with a constant width is present. Furthermore, the geometry of the narrowed region of the specimen can be considered as a notch, which produces a complex local stress field and makes the test not comparable to standard tensile testing [20]. At the end regions of the specimen, the contour widens to enable a form-fit connection with an individually machined adapter, as shown in Fig. 1b). This adapter-specimen connection allowed the integration of the small weld metal region of interest into the tensile testing machine illustrated in Fig. 1c).

This 20 kN testing device was set up at beamline P07b (PETRA III) at the synchrotron facility DESY (German: *Deutsches Elektronen-Synchrotron*) in Hamburg, Germany [21]. The tensile test was performed with a constant crosshead displacement of 8×10^{-4} mm s^{-1}. Simultaneously, a monochromatic beam with an average energy of 87.1 keV was transmitted through the specimen at the position marked in Fig. 1a). Diffractograms were taken every 5 s which is equivalent to an increase of stress less than 10 MPa during the elastic regime. In addition to the *in situ* diffraction analysis during tensile testing, two-dimensional HEXRD maps were recorded before and after testing the specimen. For the post-test investigation, the fracture halves were simply clamped together to approximate the original alignment. The specimen was scanned in both x- and y-direction with a beam size of 0.5 mm × 0.5 mm. All diffractograms were recorded using a PerkinElmer XRD 1621 flat panel detector with 2048 × 2048 pixels, each with a pitch of 200 µm. The setup was calibrated using a LaB_6-powder-standard as reference material. The following analysis was performed using the Python package pyFAI [22] for azimuthal integration and the software Profex [23] for Rietveld refinement.

3. Results

The RA scan of the specimen prior to testing is given in Fig. 2a). By comparing this scan with the entire multipass weld metal in Fig. 1a), which relies on data from Ref. [17], we can confirm the upper region at the notch as the last bead. In Fig. 2b) the absolute RA values of the scan in Fig. 2a) were subtracted by the values measured after the tensile test. Consequently, Fig. 2b) represents a two-dimensional map of the RA which mechanically transforms during tensile testing. According to this image, up to 3.5 wt.% RA can vanish. The location of the most severe transformation is in the notch region containing the last bead, marked

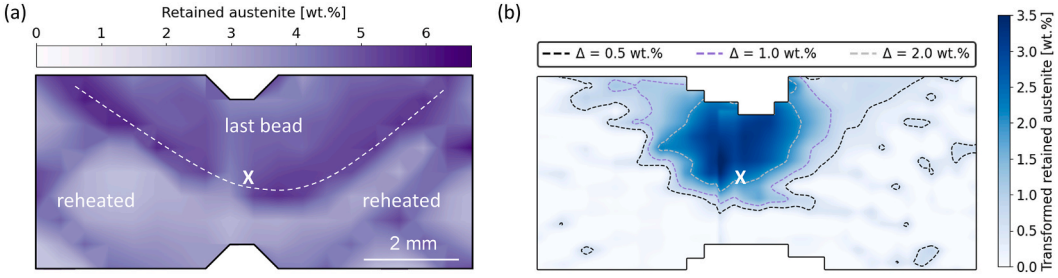

Fig. 2. a) Two-dimensional RA phase map of the tensile specimen before applying the mechanical load. **b)** Two-dimensional map of the RA transformed during the tensile test. The dashed lines indicate regions with the corresponding amount of transformed retained austenite. The cross marks the approximate location of the *in situ* HEXRD measurement.

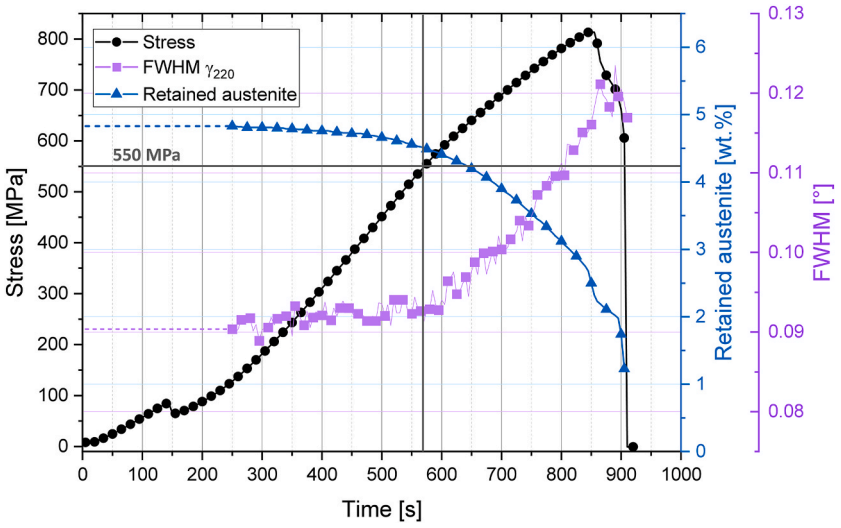

Fig. 3. Stress over time curve with the *in situ* FWHM of the austenitic γ_{220} peak and the *in situ* RA content.

by the grey dashed 2 wt.% threshold line. However, also in the unnotched region a significant transformation appears as marked by the black dashed 0.5 wt.% threshold line. This transformation only occurs in the last bead region of the tensile specimen. In the region where the weld metal is reheated by subsequent welding beads, as marked in Fig. 2a), RA is almost completely stable in the notched and notch-free part, as shown in Fig. 2b).

To correlate the RA transformation with the applied stress level (determined as the force divided by the initial cross section) and the macroscopic deformation regime (elastic or plastic), single-point *in situ* HEXRD measurements during tensile testing were performed within the region with the highest RA content. As shown in Fig. 2a), this region corresponds to the last bead, which underwent plastic deformation before fracture, as illustrated in Fig. 2b). Fig. 3 represents the corresponding stress over time curve. The purple data set in this diagram shows an overlay with the full width at half maximum (FWHM) of the austenitic γ_{220} peak, which was evaluated for a 10° segment parallel to loading direction. This FWHM starts to increase at approximately 550 MPa, which is typically associated with the accumulation of lattice defects and hence indicates the onset of plastic deformation [24]. This onset is additionally confirmed by the subtle deviation in curvature of the stress curve in the diagram. The blue data set shows an overlay with the RA fraction. Below 550 MPa, only minor RA transformation occurs, while a pronounced decrease is observed within the plastic regime. The non-linear behavior up to frame 50 and the small kink observed in the stress curve are a known characteristic of the used tensile testing machine and have been noticed in former research works [25–27]. Consequently, data up to this point were excluded from the analysis.

4. Discussion

The RA transformation in the last bead to the left and the right of the notch (Fig. 2) can be attributed to the early onset of plastic deformation, at approximately 550 MPa (Fig. 3). Since 815 MPa represents the highest stress level before fracture, the region adjacent to the notch experiences a macroscopic stress of 611 MPa due to the specimen geometry, which is sufficient to initiate plastic deformation. In the reheated weld metal, almost no RA transformation is observed in either the notched or the notch-free region. This behavior results from the presence of microalloying elements such as V, which promote precipitation hardening during the reheating from subsequent beads [28,29]. For the present alloy, a yield strength level above 1100 MPa is achieved in the multipass weld metal using standard tensile testing [17], which is significantly above the maximum stress of 815 MPa determined for the notched specimen in this study. According to Wang et al. [20], the presence of a sharp notch generally reduces ductility but increases fracture strength. Therefore, in the present case, the notched specimen would be expected to exhibit a higher strength level compared to a standard tensile test specimen. However, the early onset of plastic deformation in the last bead, caused by the absence of precipitates, lead to the opposite behavior here. These findings highlight the critical role of multipass welding in weld metals strengthened with microalloying elements. Single-pass welds exhibit a significantly lower yield strength which can lead to drastic failures in service if this limitation is not recognized [28].

As reported in many studies, the stability of RA can have an immense impact on the mechanical properties of steels. In low-alloy steels, the preferred morphology of this crucial phase for promoting toughness is film-like with a high stability [9–11]. In contrast, blocky RA is detrimental to toughness due to its early transformation under small strains [6,11]. This early onset is presumed as a result of the lower constraint and reduced C-content of blocky RA compared to film-like RA [6]. Of particular interest is whether this detrimental transformation already occurs within the macroscopic elastic regime or only after the onset of plastic deformation. Such conclusions are extensively available for TRIP steels, which contain a high amount of intentionally stabilized RA. Blonde et al. [4] and Jimenez-Melero et al. [30], for instance, described a significant transformation of austenite prior to the macroscopic yield point. For the high-strength low-alloy weld metal investigated here, such early transformation was observed only to a very small extent, although blocky RA is present in the microstructure, referred to in our previous work as stand-alone RA [17]. The dominant transformation occurs mainly in the macroscopic plastic regime.

As the strength of high-strength low-alloy steels and weld metals continues to increase, the presence of displacive microstructures with RA becomes unavoidable. Consequently, a comprehensive understanding and the control of RA morphology and stability are essential. An example is the recent work of Moon et al. [9], in which an advanced microstructure with film-like RA was achieved by intentionally alloying of high-strength steel welds. However, numerous open research questions remain about RA in low-alloy steels and weld metals. The *in situ* phase quantification performed in this study represents an important step towards a deeper understanding of the RA stability, however, a clear correlation with the microstructure is still lacking. In particular, the transformation onset for specific RA morphologies needs to be studied in more detail. It is of critical importance whether this onset occurs already in the macroscopic elastic or in the plastic regime and to what extent the specific morphologies transform during deformation. Owing to its comparatively large size and consequent ease of detection,

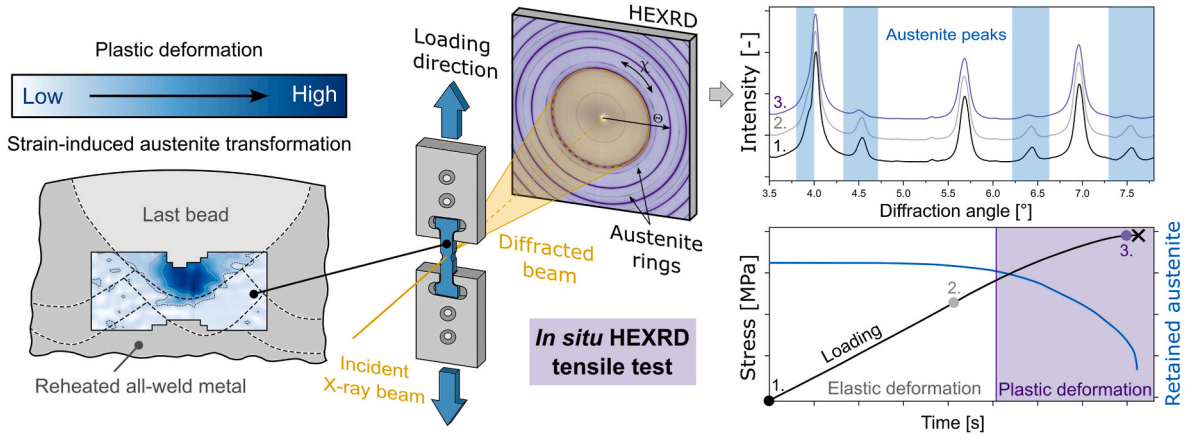

Fig. 4. Schematic representation of the methodological approach and the main findings of the present study.

blocky RA is often the focus of scientific studies, however, the *in situ* behavior of film-like RA remains insufficiently understood.

5. Conclusions

The present study investigates the strain-induced transformation of RA in a high-strength low-alloy weld metal by means of *in situ* HEXRD measurements during tensile loading, complemented by phase maps that reveal the distribution and evolution of RA. The RA remained largely stable throughout the macroscopic elastic regime, up to stress levels of approximately 550 MPa. At higher stresses, plastic deformation and RA transformation were initiated mainly within the last bead of the multipass weld metal. The reheated region remained largely unaffected, presumably due to the higher local yield strength caused by precipitation hardening. Within the notched region, the last bead area showed a pronounced decrease in RA fraction during tensile testing, from almost 5 wt.% before the tensile test to less than 1.5 wt.% after.

This study presents one of the first frameworks addressing the stability of RA in low-alloy weld metals with yield strength levels exceeding 1100 MPa. It emphasizes the importance of this metastable phase, outlines several open research questions, and proposes directions for future works. Furthermore, the results demonstrate the critical role of multipass welding when microalloying elements are employed in welding consumables to achieve effective precipitation hardening. A schematic summarizing the methodological approach and the main findings is illustrated in Fig. 4.

Credit author statement

Daniel Schrittwieser: Conceptualization, Methodology, Investigation, Writing - original draft, Writing - review & editing, Visualization, Project administration. Benjamin Seligmann: Conceptualization, Methodology, Investigation, Writing - review & editing, Visualization. David Obersteiner: Conceptualization, Methodology, Investigation, Writing - review & editing, Visualization. Sabine C. Bodner: Investigation, Writing - review & editing. Hannes Pahr: Resources, Writing - review & editing. Oleksandr Glushko: Conceptualization, Writing - review & editing. Ronald Schnitzer: Resources, Supervision, Conceptualization, Writing - review & editing.

Declaration of generative AI and AI-assisted technologies in the manuscript preparation process

During the preparation of this work the authors used ChatGPT in order to improve the readability and language. After using this tool, the authors reviewed and edited the content as needed and take full responsibility for the content of the publication.

Funding

This research did not receive any specific grant from funding agencies in the public, commercial, or not-for-profit sectors.

Declaration of competing interest

The authors declare that they have no known competing financial interests or personal relationships that could have appeared to influence the work reported in this paper.

Acknowledgements

We acknowledge DESY (Hamburg, Germany), a member of the Helmholz Association HGF, for the provision of experimental facilities. Parts of this research were carried out at PETRA III. Beamtime was allocated for proposal H-20010018. The authors would also like to thank Bruno Krajnc for the design and preparation of the unique tensile specimens. Furthermore, Maximilian Graf is acknowledged for his culinary support during the synchrotron measurements.

Data availability

Data will be made available on request.

References

[1] Nuam VL, Zhang H, Wang YC, Xiong ZP. Role of retained austenite in advanced high-strength steel: ductility and toughness. J Iron Steel Res Int 2024;31:2079–89. https://doi.org/10.1007/s42243-023-01165-3.
[2] Ryu JH, Kim DI, Kim HS, Bhadeshia HKDH, Suh DW. Strain partitioning and mechanical stability of retained austenite. Scr Mater 2010;63:297–9. https://doi.org/10.1016/j.scriptamat.2010.04.020.
[3] Soleimani M, Kalhor A, Mirzadeh H. Transformation-induced plasticity (TRIP) in advanced steels: a review. Mater Sci Eng, A 2020;795. https://doi.org/10.1016/j.msea.2020.140023.
[4] Blondé R, Jimenez-Melero E, Zhao L, Wright JP, Brück E, van der Zwaag S, et al. High-energy X-ray diffraction study on the temperature-dependent mechanical stability of retained austenite in low-alloyed TRIP steels. Acta Mater 2012;60:565–77. https://doi.org/10.1016/j.actamat.2011.10.019.
[5] Qi X, Du L, Hu J, Misra RDK. Effect of austenite stability on toughness, ductility, and work-hardening of medium-Mn steel. Mater Sci Technol 2019;35:2134–42. https://doi.org/10.1080/02670836.2018.1522088.
[6] Takahashi M, Bhadeshia HKDH. A model for the microstructure of some advanced bainitic steels. Mater Trans JIM 1991;32:689–96. https://doi.org/10.2320/matertrans1989.32.689.
[7] Bhadeshia HKDH, Edmonds DV. Bainite in silicon steels: new composition–property approach part 1. Met Sci 1983;17:411–9. https://doi.org/10.1179/030634583790420646.
[8] Miihkinen VTT, Edmonds DV. Fracture toughness of two experimental high-strength bainitic low-alloy steels containing silicon. Mater Sci Technol 1987;3:441–9. https://doi.org/10.1179/mst.1987.3.6.441.
[9] Moon J, Bae G, Jeong BY, Shin C, Kwon MJ, Kim DI, et al. Ultrastrong and ductile steel welds achieved by fine interlocking microstructures with film-like retained

austenite. Nat Commun 2024;15:1301. https://doi.org/10.1038/s41467-024-45470-1.
[10] Xie ZJ, Yuan SF, Zhou WH, Yang JR, Guo H, Shang CJ. Stabilization of retained austenite by the two-step intercritical heat treatment and its effect on the toughness of a low alloyed steel. Mater Des 2014;59:193–8. https://doi.org/10.1016/j.matdes.2014.02.035.
[11] Ding R, Tang D, Zhao A. A novel design to enhance the amount of retained austenite and mechanical properties in low-alloyed steel. Scr Mater 2014;88:21–4. https://doi.org/10.1016/j.scriptamat.2014.06.014.
[12] Li X, Shang C, Ma X, Gault B, Subramanian SV, Sun J, et al. Elemental distribution in the martensite–austenite constituent in intercritically reheated coarse-grained heat-affected zone of a high-strength pipeline steel. Scr Mater 2017;139:67–70. https://doi.org/10.1016/j.scriptamat.2017.06.017.
[13] Li X, Fan Y, Ma X, Subramanian SV, Shang C. Influence of Martensite–Austenite constituents formed at different intercritical temperatures on toughness. Mater Des 2015;67:457–63. https://doi.org/10.1016/j.matdes.2014.10.028.
[14] Schrittwieser D, Marin Morales D, Pahr H, Lumper LA, Glushko O, Schnitzer R. Microstructural insights into the coarse-grained heat-affected zone of a high-strength all-weld metal: development of a continuous cooling transformation diagram. Weld World 2025;69:813–23. https://doi.org/10.1007/s40194-024-01904-4.
[15] Bhadeshia HKDH. About calculating the characteristics of the martensite-austenite constituent. Proc Int Semin Weld High Strength Pipeline Steels, TMS 2013:99–106.
[16] Xie H, Du L-X, Hu J, Sun G-S, Wu H-Y, Misra RDK. Effect of thermo-mechanical cycling on the microstructure and toughness in the weld CGHAZ of a novel high strength low carbon steel. Mater Sci Eng, A 2015;639:482–8. https://doi.org/10.1016/j.msea.2015.05.033.
[17] Schrittwieser D, Rinnhofer N, Obersteiner D, Pahr H, Glushko O, Schnitzer R. Retained austenite in multipass high-strength weld metal with a yield strength exceeding 1100 MPa. J Mater Res Technol 2025;36:6499–505. https://doi.org/10.1016/j.jmrt.2025.04.279.
[18] Pinto LA, Pérez Escobar D, Santos OSH, Lopes NIA, Carneiro JRG, Ribeiro-Andrade R. Influence of surface preparation method on retained austenite quantification. Mater Today Commun 2020;24:101226. https://doi.org/10.1016/j.mtcomm.2020.101226.
[19] Tolchard JR, Sømme A, Solberg JK, Solheim KG. On the measurement of austenite in supermartensitic stainless steel by X-ray diffraction. Mater Char 2015;99:238–42. https://doi.org/10.1016/j.matchar.2014.12.005.
[20] Wang W, Qian X, Su R, Wang X. Tensile tests and analyses of notched specimens fabricated from high strength steels using a generalized yield model. Fatig Fract Eng Mater Struct 2010;33:310–9. https://doi.org/10.1111/j.1460-2695.2010.01443.x.
[21] Schell N, King A, Beckmann F, Fischer T, Müller M, Schreyer A. The high energy materials science beamline (HEMS) at PETRA III. Mater Sci Forum 2013;772:57–61. https://dx.doi.org/10.4028/www.scientific.net/MSF.772.57.
[22] Ashiotis G, Deschildre A, Nawaz Z, Wright JP, Karkoulis D, Picca FE, et al. The fast azimuthal integration Python library: pyFAI. J Appl Crystallogr 2015;48:510–9. https://doi.org/10.1107/S1600576715004306.
[23] Doebelin N, Kleeberg R. Profex: a graphical user interface for the Rietveld refinement program BGMN. J Appl Crystallogr 2015;48:1573–80. https://doi.org/10.1107/S1600576715014685.
[24] Ebner S, Schnitzer R, Maawad E, Suppan C, Hofer C. Influence of partitioning parameters on the mechanical stability of austenite in a Q&P steel: a comparative in-situ study. Materialia 2021;15:101033. https://doi.org/10.1016/j.mtla.2021.101033.
[25] Erdely P, Staron P, Maawad E, Schell N, Clemens H, Mayer S. Lattice and phase strain evolution during tensile loading of an intermetallic, multi-phase γ-TiAl based alloy. Acta Mater 2018;158:193–205. https://doi.org/10.1016/j.actamat.2018.07.062.
[26] Maawad E, Brokmeier HG, Zhong ZY, Al-Hamdany N, Salih M, Wagner L, et al. Determination of polycrystal diffraction elastic constants of Ti-2.5Cu by using in situ tensile loading and synchrotron radiation. Mater Sci Eng, A 2014;594:62–7. https://doi.org/10.1016/j.msea.2013.11.053.
[27] Zhong ZY, Brokmeier HG, Maawad E, Schell N. In-situ investigation of the anisotropic mechanical behavior of rolled AA 7020-T6 alloy through lattice strain evolution during uniaxial tension. Mater Sci Eng, A 2015;639:519–25. https://doi.org/10.1016/j.msea.2015.05.050.
[28] Haslberger P, Holly S, Ernst W, Schnitzer R. Precipitates in microalloyed ultra-high strength weld metal studied by atom probe tomography. Weld World 2018;62:713–9. https://doi.org/10.1007/s40194-018-0581-y.
[29] Haslberger P, Holly S, Ernst W, Schnitzer R. Microstructure and mechanical properties of high-strength steel welding consumables with a minimum yield strength of 1100 MPa. J Mater Sci 2018;53:6968–79. https://doi.org/10.1007/s10853-018-2042-9.
[30] Jimenez-Melero E, van Dijk NH, Zhao L, Sietsma J, Wright JP, van der Zwaag S. In situ synchrotron study on the interplay between martensite formation, texture evolution and load partitioning in low-alloyed TRIP steels. Mater Sci Eng, A 2011;528:6407–16. https://doi.org/10.1016/j.msea.2011.04.087.